

Electronic structure, elasticity, magnetism of Mn_2XIn(X = Fe, Co) full Heusler compounds under biaxial strain: First-principles calculations

Shiran Gao(皋世苒), Chengyang Zhao(赵成洋), Xinzhuo Zhang(张欣卓), Wen Qiao(乔文), Shiming Yan(颜士明), Ru Bai(白茹), and Tiejun Zhou(周铁军)

Citation: Chin. Phys. B, 2025, 34 (**1**): 017501. DOI: 10.1088/1674-1056/ad8ec5

What follows is a list of articles you may be interested in

Thickness-dependent magnetic property of FeNi thin film grown on flexible graphene substrate

Suixin Zhan(詹遂鑫), Shaokang Yuan(袁少康), Yuming Bai(白宇明), Fu Liu(刘福), Bohan Zhang(张博涵), Weijia Han(韩卫家), Tao Wang(王韬), Shengxiang Wang(汪胜祥), and Cai Zhou(周偲)
Chin. Phys. B, 2025, 34 (**1**): 027503. DOI: 10.1088/1674-1056/ad92fd

First-principles study of electronic and magnetic properties of Fe atoms on Cu_2N/Cu(100)

Jiale Chen(陈佳乐) and Jun Hu(胡军)
Chin. Phys. B, 2024, 33 (**8**): 087502. DOI: 10.1088/1674-1056/ad5275

Theoretical characterization of the temperature-dependent saturation magnetization of magnetic metallic materials

Jin-Long Wu(吴金龙), Pan Dong(董攀), Yi He(贺屹), Yan-Li Ma(马艳丽), Zi-Yuan Li(李梓源), Qin-Yuan Yao(姚沁远), Jun Qiu(邱俊), Jian-Zuo Ma(麻建坐), and Wei-Guo Li(李卫国)
Chin. Phys. B, 2024, 33 (**7**): 077502. DOI: 10.1088/1674-1056/ad39d1

Enhanced resonance frequency in Co_2FeAl thin film with different thicknesses grown on flexible graphene substrate

Cai Zhou(周偲), Shaokang Yuan(袁少康), Dengyu Zhu(朱登玉), Yuming Bai(白宇明), Tao Wang(王韬), Fufu Liu(刘福福), Lulu Pan(潘禄禄), Cunfang Feng(冯存芳), Bohan Zhang(张博涵), Daping He(何大平), and Shengxiang Wang(汪胜祥)
Chin. Phys. B, 2024, 33 (**3**): 037506. DOI: 10.1088/1674-1056/acfafa

Creation and annihilation of artificial magnetic skyrmions with the electric field

Jun Cheng(程军), Liang Sun(孙亮), Yike Zhang(张一可), Tongzhou Ji(吉同舟), Rongxing Cao(曹荣幸), Bingfeng Miao(缪冰锋), Yonggang Zhao(赵永刚), and Haifeng Ding(丁海峰)
Chin. Phys. B, 2024, 33 (**3**): 037501. DOI: 10.1088/1674-1056/ad188f

---

Electronic structure, elasticity, magnetism of Mn_2XIn (X = Fe, Co) full Heusler compounds under biaxial strain: First-principles calculations

Shiran Gao(皋世苒), Chengyang Zhao(赵成洋), Xinzhuo Zhang(张欣卓), Wen Qiao(乔文), Shiming Yan(颜士明)†, Ru Bai(白茹)‡, and Tiejun Zhou(周铁军)

School of Electronics and Information, Hangzhou Dianzi University, Hangzhou 310018, *China*

(Received 27 June 2024; revised manuscript received 16 October 2024; accepted manuscript online 5 November 2024)

The electronic structure, elasticity, and magnetic properties of the Mn_2XIn (X = Fe, Co) full-Heusler compounds are comprehensively investigated via first-principles calculations. The calculated elastic constants indicate that both Mn_2FeIn and Mn_2CoIn possess ductility. At the optimal lattice constants, the magnetic moments are found to be 1.40 μ_B/f.u. for Mn_2FeIn and 1.69 μ_B/f.u. for Mn_2CoIn. Under the biaxial strain ranging from −2% to 5%, Mn_2FeIn demonstrates a remarkable variation in the spin polarization, spanning from −2% to 74%, positioning it as a promising candidate for applications in spintronic devices. Analysis of the electronic structure reveals that the change in spin polarization under strain is due to the shift of the spin-down states at the Fermi surface. Additionally, under biaxial strain, the magnetic anisotropy of Mn_2FeIn undergoes a transition of easy-axis direction. Utilizing second-order perturbation theory and electronic structure analysis, the variation in magnetic anisotropy with strain can be attributed to changes of d-orbital states near the Fermi surface.

Keywords: magnetic anisotropy, biaxial strain, electronic band structure, mechanical properties

PACS: 75.30.Gw, 75.50.Cc, 75.47.Np

DOI: 10.1088/1674-1056/ad8ec5 **CSTR:** 32038.14.CPB.ad8ec5

1. Introduction

Heusler compounds, with the general formula X_nYZ (n = 1, 2), where X and Y represent transition metal elements, and Z denotes a main group element, have garnered significant attention from both theoretical and experimental perspectives for their potential applications in spintronics, energy, and magnetocaloric technologies.[1–3] Owing to their inherent compositional flexibility, Heusler compounds exhibit a diverse array of physical properties, making them viable candidates for a wide range of applications.[4,5] These include their utilization as high-temperature ferromagnetic and ferrimagnetic materials, multiferroic shape memory alloys, and topological insulators.[6–9] The current focus on the spintronic applications of Heusler compounds is primarily attributed to the observation of half-metallicity in select compounds, a phenomenon that enables the achievement of remarkable tunneling magnetoresistance at room temperature. Since the pioneering prediction by de Groot *et al*. that NiMnSb is a half-metallic ferromagnet, Heusler compounds have garnered immense interest in spintronics.[10–16]

One advantage of Heusler compounds is that most of them do not contain rare earth elements. Numerous tetragonal Heusler compounds are Mn-, Fe- or Co-based, and their magnetism is commonly ferromagnetic or ferrimagnetic. Another advantage is that a significant number of magnetic Heusler compounds exhibits gap or pseudo-gap in one spin channel, classifying them as the half-metallic materials with high spin polarization. These properties make them highly suitable for use in spintronic devices, particularly in spin valves and magnetic tunnel junctions, due to their significant potential in these research domains.[17–20] As an example, Hamaya and colleagues epitaxially grew an $Fe_{3-x}Mn_xSi$/Ge layer, which exhibited a high degree of spin polarization. This layer was then utilized as a spin injector and detector in spintronic devices based on Ge material.[21] The inherent characteristics of Heusler compounds have been shown to be modifiable, particularly through structural manipulation via the application of external strain.[22] Moreover, it has been shown that the inherent characteristics of Heusler compounds are modifiable, especially through structural manipulation via the application of external strain.[23,24] Notably, in the context of epitaxial thin films, the disparity in lattice parameters between the substrate and the film holds significant implications for the properties of the film.[25–28] Understanding the properties of Heusler compounds under different strain is of great significance for designing epitaxial thin films with specific functions. Additionally, achieving control of physical properties through strain is also beneficial for the application of Heusler compounds in spintronics. Therefore, the change of electronic structure and magnetic properties under biaxial strain for Heusler com-

†Corresponding author. E-mail: shimingyan@hdu.edu.cn

‡Corresponding author. E-mail: bairu@hdu.edu.cn

© 2025 Chinese Physical Society and IOP Publishing Ltd. All rights, including for text and data mining, AI training, and similar technologies, are reserved.

pounds is worth exploring.

The Heusler compounds Mn_2XIn (X = Fe, Co) were first predicted by Faleev recently.[29] In the report by Faleev, the lattice constants and magnetic moments of Mn_2XIn (X = Fe, Co) were examined. However, the elasticity, spin polarization and magnetic anisotropy were not explored in detail. Particularly, the tuning of these properties under strain remains poorly understood or has not been thoroughly studied. In this paper, we use first-principles calculations to determine the stable crystal structure of Mn_2XIn (X = Fe, Co). The magnetic configuration and optimal lattice constant are ascertained through calculations. The total magnetic moment of the compound with different applied biaxial strain is also predicted. The origin of magnetic moment is investigated by orbital-resolved magnetic moments. Band structure analysis is conducted to investigate the changes of spin polarization with biaxial strain. Finally, differences in magnetic anisotropy energy under various strains are calculated and analyzed using second-order perturbation theory.

2. Computational details

We used the first-principles calculations package based on density functional theory in Vienna *ab-initio* simulation package (VASP) to obtain the electronic structure, elasticity and magnetism of Mn_2XIn (X = Fe, Co) Heusler compounds.[30] The density functional theory (DFT) was employed utilizing the generalized gradient approximation (GGA) framework for calculations. The plane-wave augmented wave (PAW) pseudopotential method was utilized in conjunction with the Perdew–Burke–Ernzerhof (PBE) exchange–correlation functional. The grid division of k-point describing Brillouin zone is 9×9×9, by taking 729 k-points. The plane wave cutoff energy was set at 500 eV. The convergence criterion for the calculations was 5×10^{-2} eV/Å, ensuring that the results meet the required accuracy standards. Then, the charge density was utilized in the subsequent non-collinear calculations with spin–orbit coupling (SOC) taken into account for the magnetic anisotropy.

3. Results and discussion

3.1. Structural properties

According to the report by Faleev, structure of Mn_2XIn (X = Fe, Co) belongs to the inverse Heusler compounds consisted of four interpenetrating face-centered cubic (FCC) sublattices.[29] Figure 1 illustrates the two potential crystal structures of Mn_2XIn (X = Fe, Co) in cubic symmetry. Correspondingly, Table 1 presents the Wyckoff positions for both two possible configurations.[31,32] In theoretical calculations, there are numerous methods to assess the stability of materials, including binding energy, formation energy, phonon spectrum, molecular dynamics, and Born stability criteria, among others.[33–36] To determine whether it would be possible to synthesize the full-Heusler compound Mn_2XIn, we calculated the formation energy using the formula[37]

$$E_F(Mn_2XIn) = E_T(Mn_2XIn) - (E(Mn) + E(X) + E(In)). \quad (1)$$

In this formula, $E_T(Mn_2XIn)$ represents the energy of the chemical formula Mn_2XIn, while E(Mn), $E(X)$, and E(In) represent the energies of the free atoms Mn, X, and In, respectively. The lower the E_F, the more stable the compound is. Based on the information shown in Table 2, the formation energy of the XA–I structure is lower than that of the other type of structures for both Mn_2XIn (X = Fe, Co) compounds. This means that the XA–I structure has better thermal stability and it can be possible to prepare experimentally. All calculations will be carried out for the XA–I stable crystal structure under the $F\bar{4}3m$ space group (No. 216).

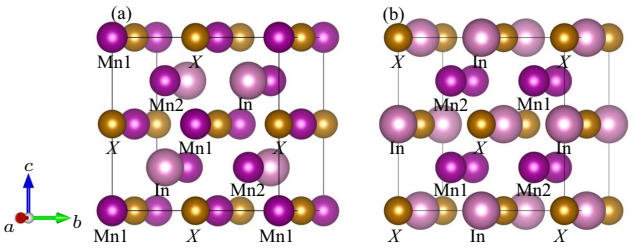


Fig. 1. Schematic representation of the possible crystal configurations of Mn_2XIn (X = Fe, Co): (a) XA–I, (b) XA–II.

Table 1. Two possible crystal configurations of Mn_2XIn (X = Fe, Co) inverse Heusler compounds.

Type	Mn1	Mn2	X	In
XA–I	A (0,0,0)	B (1/4,1/4,1/4)	C (1/2,1/2,1/2)	D (3/4,3/4,3/4)
XA–II	D (3/4,3/4,3/4)	B (1/4,1/4,1/4)	A (0,0,0)	C (1/2,1/2,1/2)

Table 2. The formation energy of two possible crystal configurations of Mn_2XIn (X = Fe, Co) inverse Heusler compounds.

Materials	Type	E_T (eV)	E_{Mn} (eV)	E_X (eV)	E_{In} (eV)	E_F (eV)
Mn_2FeIn	XA–I	–111.30	–58.15	–16.07	–7.12	–29.97
	XA–II	–110.27	–58.76	–16.09	–7.13	–28.30
Mn_2CoIn	XA–I	–107.99	–58.16	–9.40	–7.04	–33.38
	XA–II	–105.70	–58.80	–9.40	–7.04	–30.45

3.2. Magnetic properties

To determine the stable magnetic state of Mn_2XIn (X = Fe, Co), we systematically explored numerous potential magnetic configurations. This exploration involved considering diverse combinations of magnetic moment orientations for the transition metal Mn atoms. We calculated the self-consistent total energy of the compound across these varied magnetic states.[38–40] If all Mn atoms exhibit identical magnetic moment orientations, the compound is categorized as ferromagnetic (FM), as depicted in Fig. 2(a). We also evaluated antiferromagnetic (AFM) phases, considering two potential spin arrangements within the unit cell: the A-type (A-AFM) and G-type (G-AFM) antiferromagnetic structures, illustrated in Figs. 2(b) and 2(c), respectively.[41–43]

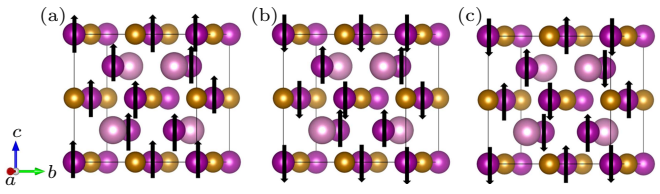


Fig. 2. Representation of three different possible magnetic states of Mn_2XIn (X = Fe, Co) inverse Heusler. The black arrow on Mn atoms represents the electron spin alignment. (a) Ferromagnetic (FM), where all Mn atoms exhibit identical magnetic moment orientations, (b) A-type antiferromagnetic (A-AFM), where the spins are aligned in the same direction in (001) plane, (c) G-type antiferromagnetic (G-AFM) compounds, where each nearest Mn atom has opposite spin.

To ascertain the equilibrium lattice constant and elucidate the relationship between the total energy and lattice constant, we undertake structural optimizations on Mn_2XIn (X = Fe, Co) compounds across three distinct magnetic structures: the FM, A-AFM, and G-AFM. Through these optimizations, we aim to pinpoint the lattice constant at which the system attains equilibrium, while concurrently discerning how the total energy varies as a function of the lattice constant. This comprehensive approach affords insights into the structural stability and energetics of Mn_2XIn compounds across different magnetic configurations. Figure 3 shows the total energy as a function of lattice parameters for the FM, A-AFM, and G-AFM magnetic structures for Mn_2XIn (X = Fe, Co). The equilibrium lattice constants, the calculated magnetic moments, and spin polarization ratios are listed in Table 3. It is clear that in all the magnetic structures, the A-AFM state shows the lower energy. Therefore, the optimal structure of Mn_2XIn (X = Fe, Co) is A-AFM structure. The optimal lattice constant of Mn_2XIn (X = Fe, Co) are 6.105 Å and 6.1 Å, which is similar to the report of Faleev.[29]

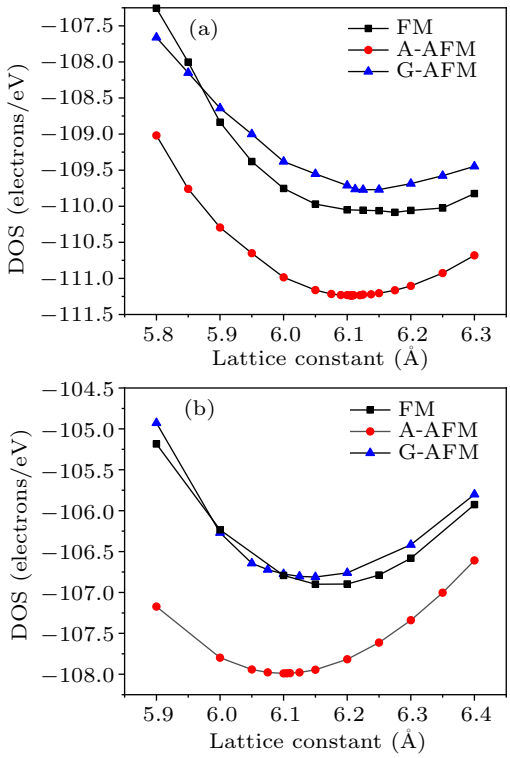


Fig. 3. Calculated total energy for Mn_2XIn (X = Fe, Co) as a function of lattice parameters for the FM, A-AFM, and G-AFM structures: (a) Mn_2FeIn, (b) Mn_2CoIn.

Table 3. The equilibrium lattice constants, total and partial magnetic moments, and spin polarization (SP) ratios of the FM, A-AFM, and G-AFM structures of Mn_2XIn (X = Fe, Co) inverse Heusler compounds (SP is obtained by Eq. (14)).

Materials	Type	Lattice constant (Å)	M_{tot} (μ_B/f.u.)	M_{Mn1} (μ_B)	M_{Mn2} (μ_B)	M_{X1} (μ_B)	M_{X2} (μ_B)	M_{In} (μ_B)	SP (%)
Mn_2FeIn	FM	6.175	8.29	3.25	2.85	2.32		0	21.0
	A-AFM	6.105	1.40	–2.97	3.05	1.34		0	26.0
	G-AFM	6.125	1.63	2.99	2.93	1.34	2.15	–0.03	3.5
Mn_2CoIn	FM	6.15	7.73	3.43	3.21	1.21		–0.12	0.6
	A-AFM	6.1	1.69	–2.70	3.32	1.07		0	4.6
	G-AFM	6.15	0	–3.20	3.21	–1.07	1.07	–0.01	0

3.3. Structural stability and elastic properties

Elastic constants provide crucial insights into the stability of any compound in response to distortion or deformation in terms of stress or strain. These constants are typically calculated using well-defined mathematical expressions[44]

$$C_{ij} = \frac{1}{V_0}\left(\frac{\partial^2 E}{\partial \varepsilon_i \partial \varepsilon_j}\right), \tag{2}$$

where, V_0 is volume in the equilibrium state, E denotes the internal energy, and ε_i and ε_j are the applied strains. The value of C_{ij} helps determine the moduli (bulk, shear, Young's) and related parameters, which relate hardness to tensile strength and indicate ductility, brittleness, plasticity, or elasticity, among other properties.[45] Born stability condition plays an important role in the determination of mechanical stability.

To calculate these elastic constants, we use the following method: apply a series of small strains from −0.015 to 0.015 in 0.005 steps to the optimized unit cell, and then calculate the corresponding stresses. This process is designed to simulate the response of a material to a small deformation in order to accurately determine its elastic properties.

In the present study, we have employed a method pioneered by Thomas Charpin and integrated into VASKPIT to calculate elastic constants C_{11}, C_{12}, and C_{44}.[46] Bulk modulus (B), shear modulus (G), Young modulus (E), Poisson's coefficient (P_0), anisotropy (A), longitudinal, transverse, and mean velocities (v_t, v_l, and v_m), and Debye temperature (θ_D) have been computed using the following equations:[44,47]

$$B = \frac{1}{3}(C_{11} + 2C_{12}), \tag{3}$$

$$G_{\rm V} = \frac{C_{11} - C_{12} + 3C_{44}}{5},$$

$$G_{\rm R} = \frac{5C_{44}(C_{11} - C_{12})}{4C_{44} + 3(C_{11} - C_{12})}, \quad G = \frac{G_{\rm V} + G_{\rm R}}{2}, \tag{4}$$

$$E = \frac{9BG}{B+G}, \tag{5}$$

$$P_0 = \frac{3B - 2B}{2(3B+G)}, \tag{6}$$

$$A = \frac{2C_{44}}{C_{11} - C_{12}}, \tag{7}$$

$$v_{\rm l} = \left(\frac{3B+4G}{3\rho}\right)^{1/2}, \tag{8}$$

$$v_{\rm t} = \left(\frac{G}{\rho}\right)^{1/2}, \tag{9}$$

$$v_{\rm m} = \left(\frac{1}{3}\left(\frac{2}{v_{\rm t}^3} + \frac{1}{v_{\rm l}^3}\right)\right)^{-1/3}, \tag{10}$$

$$\theta_{\rm D} = \frac{h}{k_{\rm B}}\left(\frac{3n}{4\pi V_{\rm a}}\right)^{-1/3} v_{\rm m}. \tag{11}$$

The symbols ρ, h, $k_{\rm B}$, n, and $V_{\rm a}$, respectively, represent the density, Planck's constant, Boltzman's constant, number of atoms per formula unit, and the atomic volume of the alloy.[48–50]

Table 4. Calculated bulk modulus (B) and elastic constants (C_{11}, C_{12}, and C_{44}) for Mn_2XIn (X = Fe, Co) by HILL approach and longitudinal, transverse, and average sound velocity ($v_{\rm l}$, $v_{\rm t}$, and $v_{\rm m}$) with Debye temperature ($\theta_{\rm D}$).

Parameters	Fe	Co
C_{11}	121	113
C_{12}	112	98
C_{44}	93	93
$C_{11} - C_{12}$	9	15
$C_{11}+2C_{12}$	345	309
Bulk modulus B_0 (GPa)	115	103
$G_{\rm V}$	58	59
$G_{\rm R}$	10	16.73
Shear modulus G (GPa)	34	38
Young modulus E (GPa)	93	101
Elastic anisotropy A	20.67	12.40
Poisson's coefficient P_0	0.37	0.34
Cauchy's pressure P	19.00	5.00
Pugh's ratio B_0/G	3.38	2.73
Poisson's ratio v	0.29	0.33
Longitudinal velocity $v_{\rm l}$ (m·s^{-1})	4565	4173
Transverse velocity $v_{\rm t}$ (m·s^{-1})	2498	2116
average sound velocity $v_{\rm m}$ (m·s^{-1})	2785	2371
Debye temperature $\theta_{\rm D}$ (K)	342	292

In the current investigation, the cubic symmetry of the alloys constrains the number of independent elastic parameters to three (C_{11}, C_{12}, and C_{44}). These parameters, along with other elastic properties derived from them, are computed using Eqs. (2)–(10) and summarized in Table 4. It is noted that the Mn_2XIn (X = Fe, Co) compounds satisfy the mechanical stability criteria (named as Born–Huang criteria) for a cubic crystal in the $F\bar{4}3m$ configuration, which are $C_{11} > 0$, $C_{12} > 0$, $C_{11} - C_{12} > 0$, and $C_{11} + 2C_{12} > 0$.[51]

The Poisson's ratio (v), defined as the ratio of transverse strain to longitudinal strain along the direction of elastic loading, provides profound insights into the underlying bonding properties of solids.[52,53] Generally, covalent materials exhibit a Poisson's ratio of roughly 0.1, whereas ionic materials possess a ratio of 0.25. Metals, on the other hand, occupy a range from 0.28 to 0.42.[54] Remarkably, the Mn_2XIn compound demonstrates a Poisson's ratio spanning from 0.29 to 0.33, indicating the presence of distinctive metallic bonding characteristics within its structure.

To further analyze the ductile or brittle nature of materials, there are three criteria considered: Cauchy's pressure P, Pugh's ratio B_0/G, and Poisson's coefficient P_0. Cauchy's pressure ($P = C_{12} - C_{44}$) for Mn_2XIn (X = Fe, Co) is positive, suggesting a ductile tendency in these compounds.[55] The values of Pugh's ratio (B_0/G), calculated as 3.38 for Mn_2FeIn and 2.73 for Mn_2CoIn, exceed the critical value of 1.75, which serves as a threshold for distinguishing ductile and brittle materials.[56–58] Additionally, the Poisson's coefficients of 0.37 for Mn_2FeIn and 0.34 for Mn_2CoIn are higher than the critical value of 0.26, further confirming the ductile nature of Mn_2XIn.

The calculated values of the anisotropy factor A for Mn_2XIn increase when X changes from Fe to Co, attributed to the increasing atomic radius.[59] This increase in A values also indicates a high degree of elastic anisotropy in these materials.

Based on the analyses, we can confidently assert that the Mn_2XIn (X = Fe, Co) compound possesses superior ductility. This characteristic suggests that the lattice mismatch encountered during the fabrication of heterojunction and spintronic devices using Mn_2XIn is unlikely to cause significant damage to the devices. To gain a deeper understanding of how lattice mismatch affects the material's properties, we will proceed to investigate the changes in Mn_2XIn's electronic structure, spin characteristics, and magnetic anisotropy under biaxial strain conditions.

3.4. Electronic structure, magnetic properties under biaxial strain

3.4.1. Electronic structure and magnetic moments

As the Slater–Pauling curve (SPC), the magnetic moment per unit cell, expressed in multiples of Bohr magneton (in units of $\mu_{\rm B}$/f.u), is delineated by a relationship[60,61]

$$M_{\rm total} = N - 24. \tag{12}$$

The variable N represents the count of valence electrons contained within the unit cell. For Mn_2FeIn, there are a total of 25 $(2\times7+8+3)$ valence electrons. For Mn_2CoIn, there are a total of 26 $(2\times7+9+3)$ valence electrons. For this reason, the magnetic moment expected from SPC is 1 $\mu_{\rm B}$/f.u for

Mn_2FeIn and 2 μ_B/f.u. for Mn_2CoIn. The calculated values of total and individual magnetic moments at the equilibrium lattice constants for Mn_2XIn (X = Fe, Co) are shown in Fig. 4. The calculated magnetic moment of Mn_2FeIn is 1.40 μ_B/f.u. and Mn_2CoIn is 1.69 μ_B/f.u. Faleev *et al.* have also reported the magnetic moment of Mn_2XIn (X = Fe, Co) to be 1.26 μ_B/f.u. and 1.87 μ_B/f.u., respectively.[29] To further elucidate this phenomenon, we have analyzed and presented the trends in total and partial magnetic moments under varying strain conditions, as depicted in Fig. 4. The strain is calculated as $(a_0 - a)/a_0 \times 100\%$, where a represents the current lattice constant on the biaxial axis, and a_0 denotes the equilibrium lattice constant.

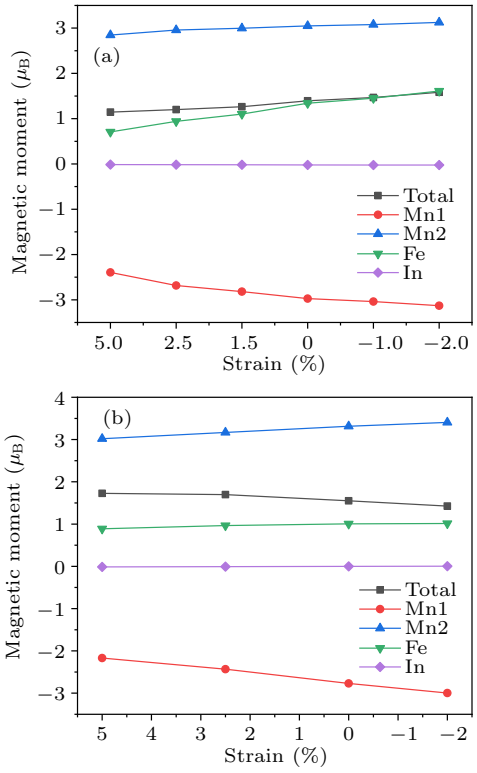


Fig. 4. Variations of magnetic moment and spin polarization with variation under biaxial strain for (a) Mn_2FeIn and (b) Mn_2CoIn.

As the strain decreases, magnetic moment of Fe and Mn2 in Mn_2FeIn increases, while the magnetic moment of Mn1 decreases. Based on the simplified rigid band model, the emergence of magnetic moments stems from the difference in density of states (DOS) between the spin-majority and spin-minority bands. The PDOS (partial density of states) for the Fe, Mn2, and Mn1 atoms were calculated and plotted in Figs. 5 and 6.

Combined with data of the DOS, there is degeneracy in the d_{yz} and d_{xz} orbitals of the two atoms (Fe and Mn2). As shown in Fig. 5, With the decrease of biaxial strain, the proportion of the spin-up d_{xy}, d_{yz} (d_{xz}), and d_{z^2} orbitals of Fe in the occupied state increases with the trend of the movement to the state of lower energy and there is no significant change in the proportion of spin- down d_{xy} and d_{yz} (d_{xz}) orbitals which results in an increase in the magnetic moment of these orbitals. Meantime, the proportion of the spin-down d_{z^2} orbital in the occupied state decreases with the movement to the state of higher energy which results in the increase of the total magnetic moment of the d_{z^2} orbitals. As a result, the magnetic moment of the Fe atom increases with the decrease of strain. In terms of magnetic moment, the Mn2 atom has a similar tendency with the Fe atom. As shown in Fig. 5 (right), the spin-up $d_{x^2-y^2}$ and d_{yz} (d_{xz}) orbitals of Mn2 atoms move towards the state of lower energy, resulting in the increasing proportion of occupied states and the increasing magnetic moment of the spin-up. The proportion of spin-down occupied states diminishes due to the movement of the spin-down $d_{x^2-y^2}$ orbitals to the higher energy state. This results in the increase in the proportion of the spin-down unoccupied orbitals near the Fermi surface, while the proportion of occupied states decreases. As a result, the orbital magnetic moment contributed by the spin-up contribution of the Mn2 atom increases and the magnetic moments contributed by the spin-down decreases, and finally the total magnetic moment of the Mn2 atom increases.

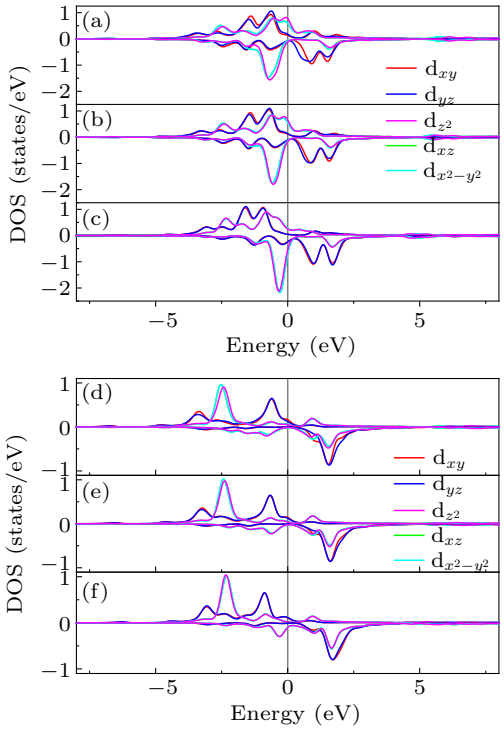


Fig. 5. PDOS of Fe [(a)–(c)] and Mn2 [(d)–(f)] for Mn_2FeIn under different biaxial strain at 5% in panels (a) and (d), 2.5% in panels (b) and (e), and −2% in panels (c) and (f).

Similarly, in Fig. 6, the proportion of spin-up unoccupied state increases due to the movement toward the state of the higher energy of d_{xy}, d_{z^2}, d_{xz}, and $d_{x^2-y^2}$ orbitals of Mn1 for Mn_2CoIn with the decrease of biaxial strain, while the spin-down occupied proportion of d_{xy}, d_{z^2}, d_{xz}, and $d_{x^2-y^2}$ orbitals decreases which result in an increase of the magnetic moments contributed by the spin-down contribution and the decrease of

the magnetic moments contributed by the spin-up, and finally lead to the decrease of total magnetic moment of the Mn1 atom.

According to the formula for calculating the orbital magnetic moment:

$$M = \frac{\int_{E_{\mathrm{MIN}}}^{E_{\mathrm{f}}} N^{\uparrow}(E)\,\mathrm{d}E}{\int_{E_{\mathrm{MIN}}}^{E_{\mathrm{MAX}}} N^{\uparrow}(E)\,\mathrm{d}E} - \frac{\int_{E_{\mathrm{MIN}}}^{E_{\mathrm{f}}} N^{\downarrow}(E)\,\mathrm{d}E}{\int_{E_{\mathrm{MIN}}}^{E_{\mathrm{MAX}}} N^{\downarrow}(E)\,\mathrm{d}E}, \tag{13}$$

where E_{f} is the energy of Fermi level, E_{MAX} and E_{MIN} refer to lowest and highest energies of density of states, and $N(E)$ refers to the distribution of density of states with energy. We calculated the magnetic moments of the orbitals in atoms based on data of DOS, and organized to Table 5 as shown below.

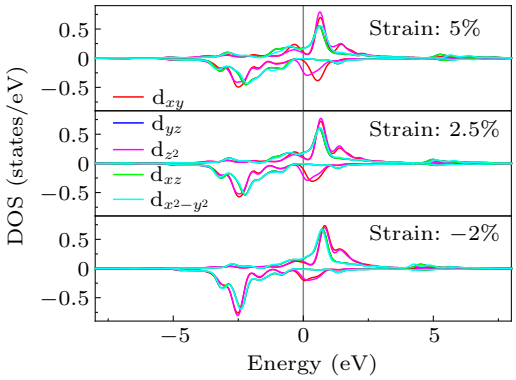


Fig. 6. PDOS of Mn1 for Mn_2CoIn under different biaxial strains at 5%, 2.5%, and −2%.

Table 5. The magnetic moment and the total magnetic moment of atomic orbital.

Materials	Atom	Strain (%)	$M_{d_{xy}}$ (μ_B)	$M_{d_{yz}}$ (μ_B)	$M_{d_{z^2}}$ (μ_B)	$M_{d_{xz}}$ (μ_B)	$M_{d_{x^2-y^2}}$ (μ_B)	M_{tot} (μ_B)
Mn_2FeIn	Fe	5	0.36	–0.03	0.42	–0.03	–0.06	0.66
		2.5	0.43	–0.01	0.46	–0.01	–0.02	0.85
		–2	0.57	0.11	0.55	0.11	0.11	1.45
	Mn1	5	–0.41	–0.45	–0.45	–0.45	–0.51	–2.27
		2.5	–0.48	–0.50	–0.50	–0.50	–0.53	–2.53
		–2	–0.60	–0.59	–0.59	–0.59	–0.57	–2.94
	Mn2	5	0.74	0.41	0.76	0.41	0.42	2.74
		2.5	0.74	0.44	0.75	0.44	0.45	2.82
		–2	0.75	0.49	0.74	0.49	0.49	2.96
Mn_2CoIn	Co	5	0.34	0.06	0.35	0.06	0.05	0.87
		2.5	0.38	0.06	0.38	0.06	0.08	0.95
		–2	0.42	0.06	0.41	0.06	0.06	1.01
	Mn1	5	–0.36	–0.43	–0.46	–0.43	–0.49	–2.17
		2.5	–0.45	–0.49	–0.51	–0.49	–0.52	–2.46
		–2	–0.64	–0.61	–0.60	–0.61	–0.59	–3.05
	Mn2	5	0.80	0.48	0.82	0.48	0.50	3.01
		2.5	0.82	0.53	0.83	0.53	0.54	3.24
		–2	0.85	0.60	0.85	0.60	0.60	3.50

Based on the comprehensive analysis and calculation results, the variation of atomic magnetic moments under strain originates from changes in the proportion of d-orbital states.

3.4.2. Spin polarization

Based on the total DOS data, we calculated the spin polarizability exhibited by the material under different strains. The electron spin polarization (SP) at Fermi surface of a material is defined as follows:[22,62–66]

$$\mathrm{SP} = \frac{\rho^{\uparrow}(E_{\mathrm{F}}) - \rho^{\downarrow}(E_{\mathrm{F}})}{\rho^{\uparrow}(E_{\mathrm{F}}) + \rho^{\downarrow}(E_{\mathrm{F}})} \times 100\%, \tag{14}$$

where $\rho^{\uparrow}(E_{\mathrm{F}})$ and $\rho^{\downarrow}(E_{\mathrm{F}})$ are the majority and minority densities of states at Fermi surface. Compounds are considered to be genuine half-metals when the SP value reaches 100%, which occurs when either the density of states (DOS) from the majority or minority spins is precisely zero at the energy level of the Fermi surface, while the other DOS remains non-zero. Calculated SP for Mn_2FeIn and Mn_2CoIn with the strain from −2% to 5 % is shown in Fig. 7.

It becomes evident that the SP of Mn_2FeIn can be enhanced by tensile strain. As strain varies from −2% and 5%, Mn_2FeIn exhibits a remarkable SP variation from −2% to 74% and Mn_2CoIn exhibits a relatively gradual SP variation from −8% to 13%.

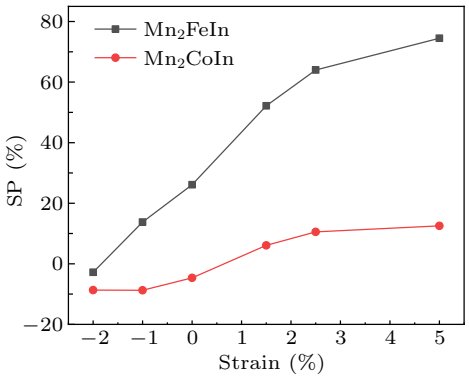


Fig. 7. Variations of spin polarization (SP) with strain for Mn_2FeIn and Mn_2CoIn.

We depicted the total and partial DOS under different biaxial strain, as shown in the Fig. 8. Fe and Co atoms play a

dominant role in the total spin down state on the Fermi level. Under the strain of 5%, the spin-down DOS exhibits a very low proportion on the Fermi surface in Mn_2FeIn. Furthermore, according to the detailed data of DOS, it can be known that the proportion of the density of states here is about 0.9, Thus, the pseudo-band gap here is the main reason for the large change of spin polarization in Mn_2FeIn with strain.

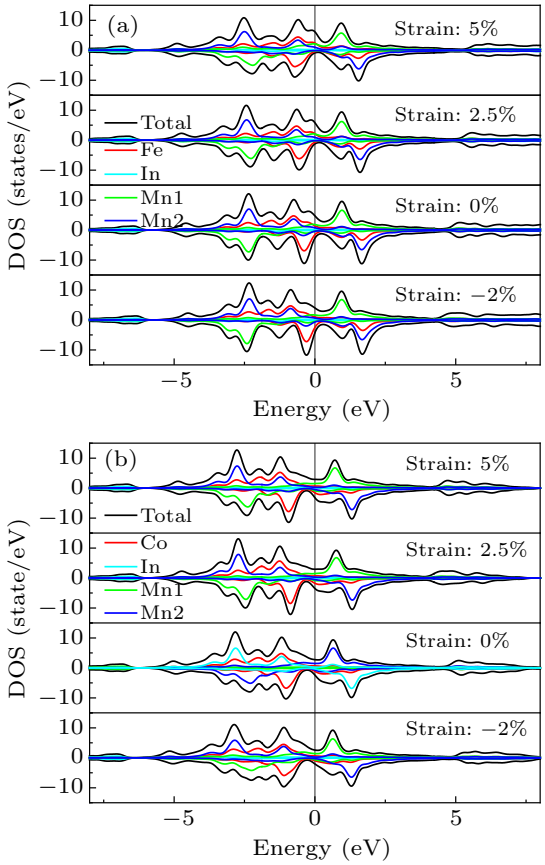


Fig. 8. Plots of total and partial DOSs under different strains: (a) Mn_2FeIn and (b) Mn_2CoIn.

We further explore, from the band structure, the variation of the spin polarization of Mn_2FeIn with strain of 5% and −2%. As shown in Fig. 9, under the strain of −2%, the band structures are observed to show metallic behavior for majority spins and minority spins, which are in good agreement with the DOS (Fig. 8(a)). With the increase of strain, the energy bands at the Fermi surface for minority spin move towards the occupied state, and the band shapes at the K points of 1/2 of L–Γ and 1/2 of Γ–X become steeper and show the tendency to be more close to K point of Γ. Meanwhile the band gap at other K points increases, resulting in a decrease in the proportion of electron energy states at the Fermi surface and the appearance of pseudo-band gap (still metallic) in DOS.

Then, to further understand the d-orbital distribution around Fermi surface and the effect of strain, we plotted the d-orbital splitting and partial DOS of Mn and Fe atoms in the Mn_2FeIn compound, as shown in Figs. 10 and 11, respectively.

In Fig. 10, we have elucidated the plausible hybridization of d electrons occurring between Fe and Mn atoms within Mn_2FeIn. The d orbitals associated with Fe and Mn are partitioned into threefold-degenerate t_{2g} states (d_{xy}, d_{yz}, d_{zx}) and twofold-degenerate e_g states ($d_{x^2-y^2}$, d_{z^2}).[51] To explicate the hybridization process, we initially examine the d states of Mn1 and Mn2 atoms. Following the hybridization of these states, a set of five bonding and antibonding states emerge, comprising ($2\times e_g$ and $3\times t_{2g}$) and ($2\times e_u$ and $3\times t_{1u}$), respectively. Subsequently, the newly formed states resulting from the Mn1–Mn2 hybridization interact with the t_{2g} and e_g states of Fe, thereby yielding ten states (comprising five bonding and five antibonding states). However, it is noteworthy that the antibonding states ($2\times e_u$ and $3\times t_{1u}$) originating from the Mn1–Mn2 hybridization cannot effectively couple with the d orbitals of Fe. This limitation arises from the fact that Fe solely possesses e_g and t_{2g} states, thus underscoring its role in establishing the d–d band gap.[67]

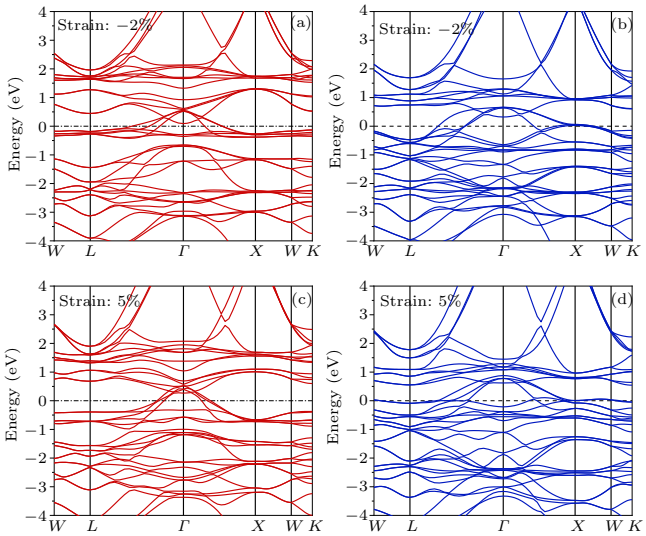


Fig. 9. Band structures: majority spin (red lines) and minority spin (blue lines) of Mn_2FeIn under the strain of −2% [(a) and (b)] and 5% [(c) and (d)].

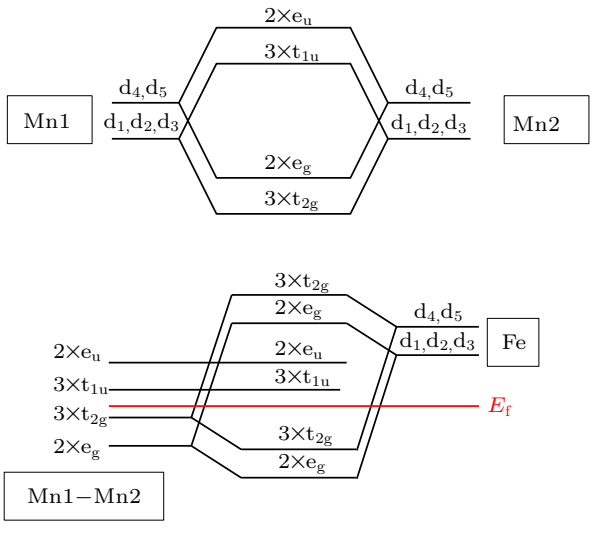


Fig. 10. Splitting of d-orbital in Mn_2FeIn Heusler compounds.

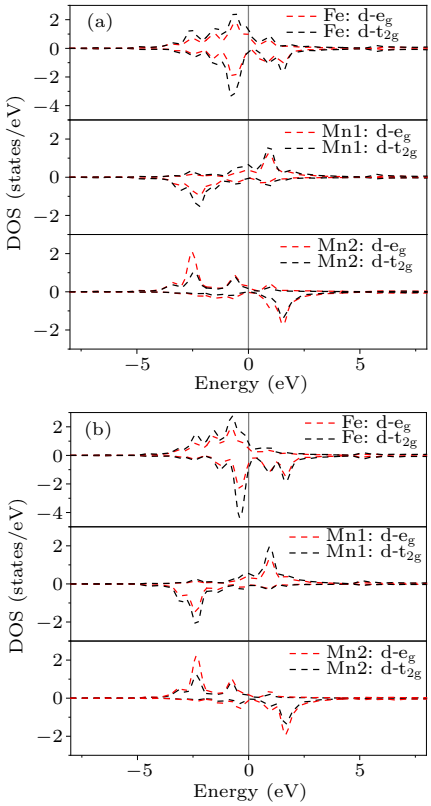


Fig. 11. Partial DOS of d-orbital for the Mn_2FeIn with the strain of (a) 5% and (b) 0%.

Figure 11 shows the DOS for each atom with and without strain. From Fig. 11, it is evident that in majority spin PDOS, e_g electrons and t_{2g} electrons of Fe and Mn1 highly contribute at E_F for Mn_2FeIn. In minority spin PDOS, the proportion at the Fermi surface is mainly due to the contribution of t_{2g} electrons of the Fe atom. With the effect of the strain, the spin-down d-e_g electrons of Fe move toward the lower energy of the state and lead to the decrease for the proportion the total spin-down DOS, thus leading to a very large variation in SP.

3.4.3. Magnetic anisotropy

The magnetic anisotropic energy (MAE) is defined as the energy difference for the magnetization along the arbitrary direction [a b c] and perpendicular [0 0 1] direction.[68,69] The SOC included in the noncollinear calculations using the second variation method is considered for calculating the MAE:[70–73]

$$\mathrm{MAE}_{[a\ b\ c]} = E_{[a\ b\ c]} - E_{[0\ 0\ 1]}. \tag{15}$$

According to the second-order perturbation theory, the energy state distribution of atomic orbital at the Fermi surface will cause changes in the magnetic anisotropy of the material. The MAE under different strains for Mn_2XIn is shown in Table 6.

From the results in the above table, it can be concluded that the easy axis corresponding to the lowest energy point of Mn_2FeIn under different strains is transformed between [001] and [100], indicating that the magnetic orientation of Mn_2FeIn is sensitive to strain, while Mn_2CoIn exhibits a stable in-plane MA, indicating that it is not strain-sensitive. Subsequently, we began to explore the principle of the easy axial transition of Mn_2FeIn under different strains. Firstly, we explored the change in the $\mathrm{MAE}_{[100]}$ of each atom under different strains through atom-resolution as shown in Fig. 12.

The change in MA is mainly due to the Fe and Mn1 atoms in layer II. Under the strain of 5% to −2%, both Fe and Mn1 atoms undergo a transition from in-plane MA to out-of-plane MA.

Table 6. The calculated $\mathrm{MAE}_{[a\ b\ c]}$ (in unit eV) in Mn_2XIn (X = Fe, Co) under different effects of the strain. The MAE in bulk Mn_2FeIn and Mn_2CoIn are listed for comparisons.

Materials	Strain (%)	$E_{[001]}$ (eV)	$\mathrm{MAE}_{[100]}$ (meV)	$\mathrm{MAE}_{[101]}$ (meV)	$\mathrm{MAE}_{[110]}$ (meV)	$\mathrm{MAE}_{[111]}$ (meV)	Easy axis
Mn_2FeIn	5	−55.30	1.86×10^{-1}	9.34×10^{-2}	1.85×10^{-1}	1.24×10^{-1}	[001]
	0	−55.80	–	-5.45×10^{-2}	-1.07×10^{-1}	-7.20×10^{-2}	[110]
	−2	−55.76	-1.70×10^{-2}	-9.08×10^{-3}	-1.61×10^{-2}	-1.15×10^{-2}	[100]
Mn_2CoIn	5	−53.72	2.23×10^{-1}	1.11×10^{-1}	2.22×10^{-1}	1.48×10^{-1}	[100]
	0	−54.16	–	2.86×10^{-3}	4.94×10^{-3}	3.57×10^{-3}	[100]/[001]
	−2	−54.10	-1.07×10^{-1}	-5.33×10^{-2}	-1.07×10^{-1}	-7.11×10^{-2}	[100]

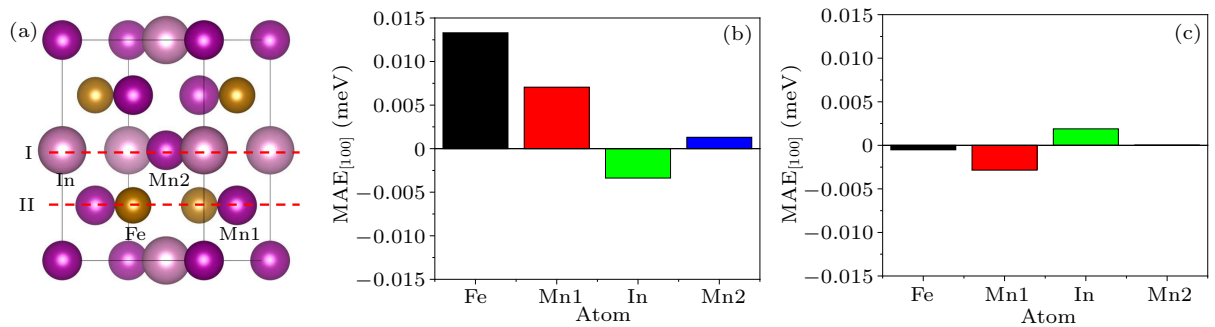


Fig. 12. (a) Structural diagram of Mn_2FeIn, MAE [100] of each atom under the strain of (b) 5% and (c) −2%.

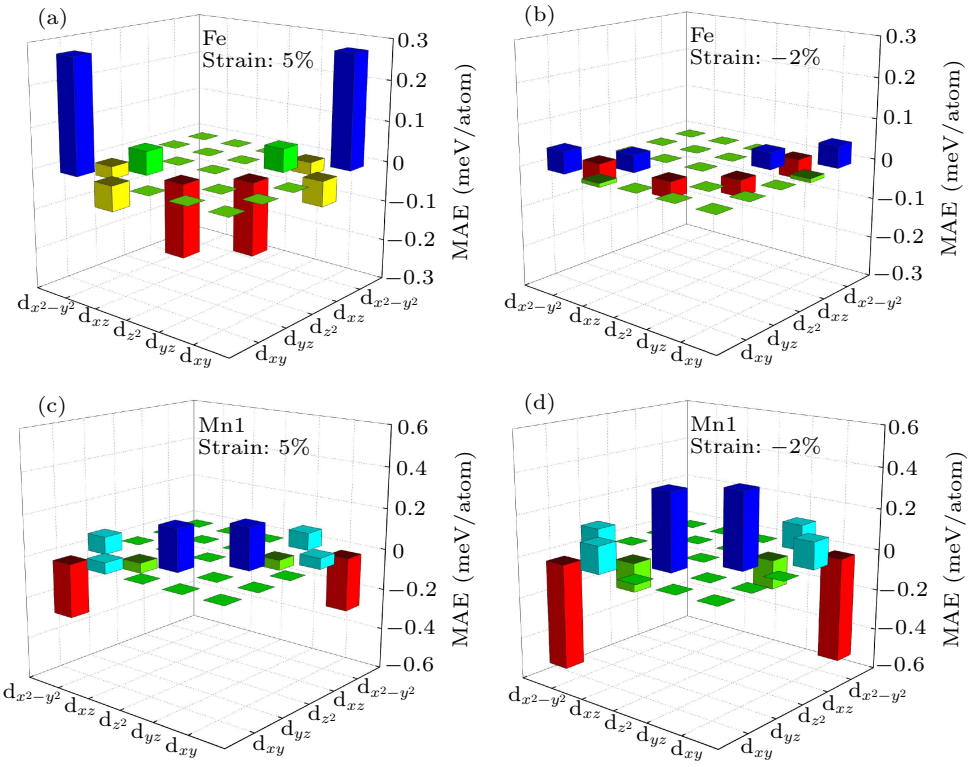


Fig. 13. The orbital-resolved MAE of the Fe and Mn1 under the strain of 5% and −2%.

We have calculated the orbital-resolved MAE of the Fe and Mn1 atom located in the layer II of Mn_2FeIn. As shown in Fig. 13, when the strain is 5%, the interaction between the $d_{x^2-y^2}$ and d_{xy} orbitals ($d_{x^2-y^2}/d_{xy}$) of the Fe atom results in a significant positive contribution to its total MAE, while the MAE from the d_{z_2} and d_{yz} orbitals (d_{z_2}/d_{yz}) contributes negatively. Due to the fact that the magnitude of the positive contribution surpasses the negative one, the Fe atom exhibits a positive MAE under the strain of 5%. When the strain is −2%, the positive MAE from the $d_{x^2-y^2}/d_{xy}$ orbitals decreases, and the negative MAE from d_{z_2}/d_{yz} orbitals reduces, resulting in the rapid decrease of the total MAE of the Fe atom. Under the strain of 5%, the MAE of Mn1 atom is mainly caused by the hybridization of $d_{x^2-y^2}/d_{xy}$ orbitals and d_{z_2}/d_{yz} orbitals, and when the strain is −2%, the hybridization is weakened, so that the value of the total MAE changes from the positive to the negative.

Based on numerous theoretical investigations, the alterations in MAE are closely tied to variations in the electron occupancy of d orbitals near the Fermi level. Therefore, to deeply understand the influence of the strain on the MAE of the Fe and Mn1 atom in the layer-II, we explored the atomic d-orbital resolved PDOS, as shown in Fig. 14.

Magnetic anisotropy stems from the SOC effect, and the MAE is the consequence of the competition between in-plane and perpendicular contributions of the SOC Hamiltonian. Within the framework of the second-order perturbation theory, the MAE can be approximately expressed in terms of angular momentum operators L_x (or L_y) and L_z as[74]

$$\mathrm{MAE} \approx \xi^2 \sum_{u\alpha,o\beta} \left(2\delta_{\alpha\beta}-1\right) \times \left[\frac{|\langle u\alpha|L_z|o\beta\rangle|^2}{E_{u\alpha}-E_{u\beta}} - \frac{|\langle u\alpha|L_{x/y}|o\beta\rangle|^2}{E_{u\alpha}-E_{u\beta}}\right]. \quad (16)$$

Here ξ is the SOC constant; $E_{u\alpha}$ and $E_{o\beta}$ are the energy levels of an unoccupied state with spin α ($|u\alpha\rangle$) and an occupied state with spin β ($|o\beta\rangle$), respectively. As shown in Fig. 14, The spin conservation term of spin-up occupied $d_{x^2-y^2}$ orbital and the spin-up unoccupied d_{xy} orbital produce hybridization at the Fermi surface, resulting in an out-of-plane MAE contribution (positive contribution) to Fe atoms. With the decrease of strain, the $d_{x^2-y^2}$ orbital moves to the lowest energy state of the occupied state, resulting in a decrease in the proportion at the Fermi surface. And the d_{xy} orbital moves to the occupied state of lower-energy, resulting in a small proportion increase in the proportion at the Fermi surface. According to the second-order perturbation theory, the MAE produced by the hybridization of $d_{x^2-y^2}/d_{xy}$ orbitals decreases. When the strain is 5%, the hybridization of d_{z^2}/d_{yz} occurs mainly at the spin-up Fermi surface and results in the negative contribution. As the decrease of the strain, the proportion of d_{yz} in the spin-up occupied state and d_{z^2} in the spin-down unoccupied state increases, resulting in a positive MAE contribution.

Similarly, for Mn1 atoms, the spin flip term of SOC from $d_{x^2-y^2}$ and the d_{xy} orbital produces negative MAE, which is mainly due to the hybridization of the spin-up occupied $d_{x^2-y^2}$ orbital in the near the Fermi surface and the spin-down unoccupied d_{xy} orbital. As the strain decreases, the proportion of

the spin-down unoccupied d_{xy} orbital decreases, resulting in a decrease in the negative contribution to the MAE. The spin flip term d_{z^2} and d_{yz} orbitals have a positive contribution to the overall MAE, which is mainly derived from the hybridization of the spin-up occupied d_{yz} orbital in the near the Fermi surface and the spin-down unoccupied d_{z^2} orbital. As the proportion of d_{z^2} orbitals at the Fermi surface decreases under strain, the resulting positive contribution to MAE decreases.

It is evident from the band structure shown in Figs. 15 and 16 that the spin-up $d_{x^2-y^2}$ orbital state tends to move away from the Fermi level at the L point, while the spin-down d_{z^2} orbital state shows the same trend at the Γ point as the strain decreases for Fe in Mn_2FeIn. And according to the information of bubble diagram in the band structure, the proportion of spin-down unoccupied d_{yz} orbital of Mn1 atom along the k-point path of Γ–X decreases with the decrease of strain. These d orbitals state shifts in the energy bands are responsible for the decrease of MAE.

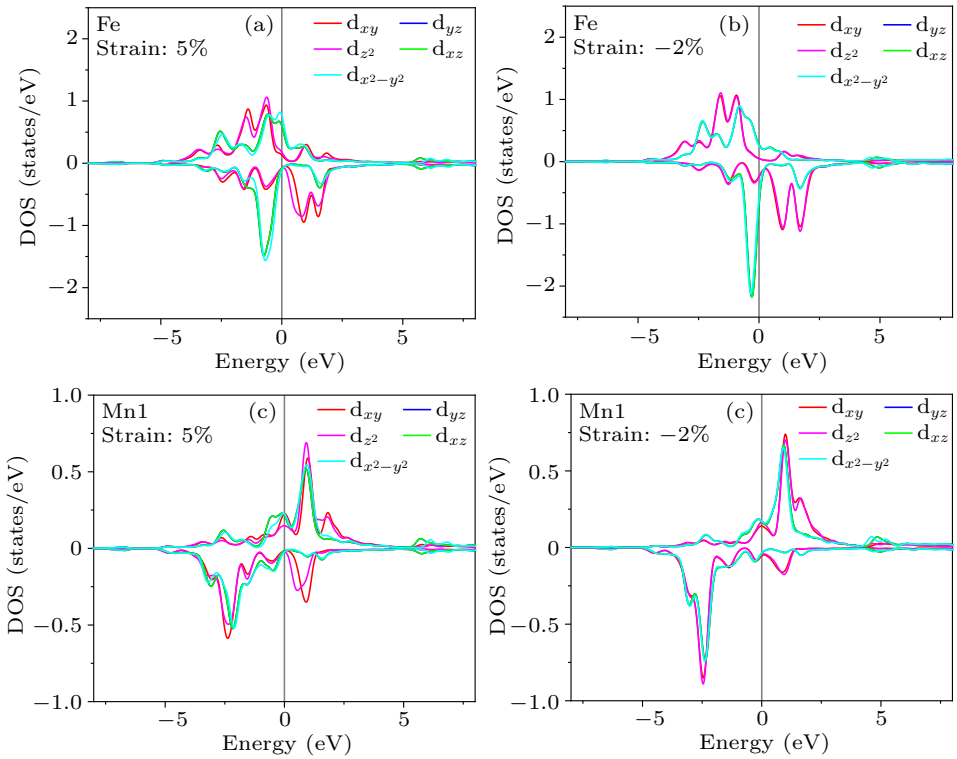


Fig. 14. The PDOSs of Fe and Mn1 atoms in the layer-II.

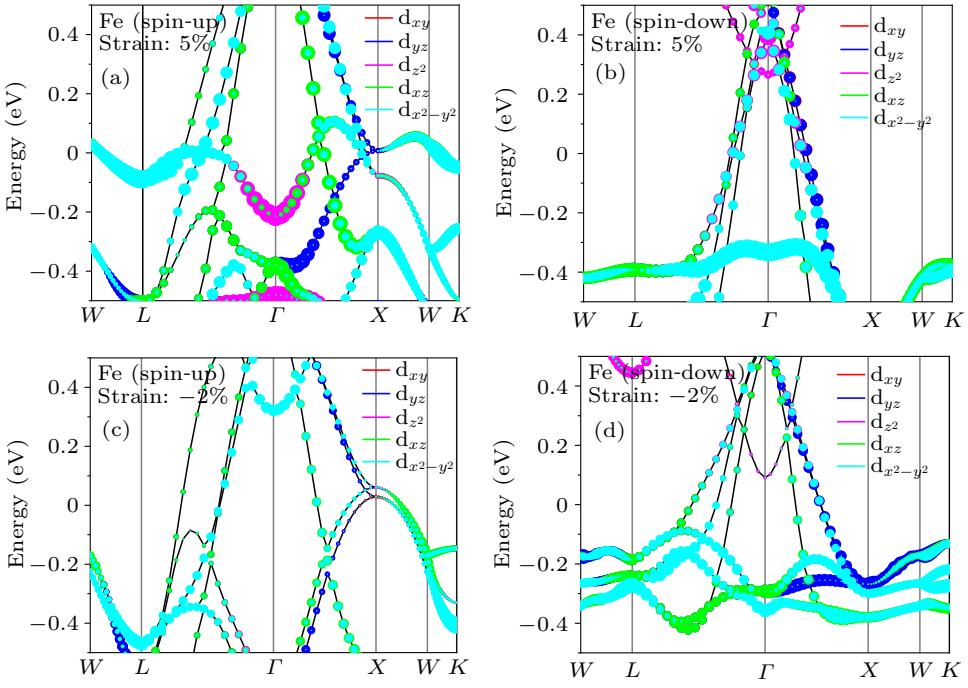


Fig. 15. The d-orbital-projected band structures of Fe in Mn_2FeIn under the different strain.

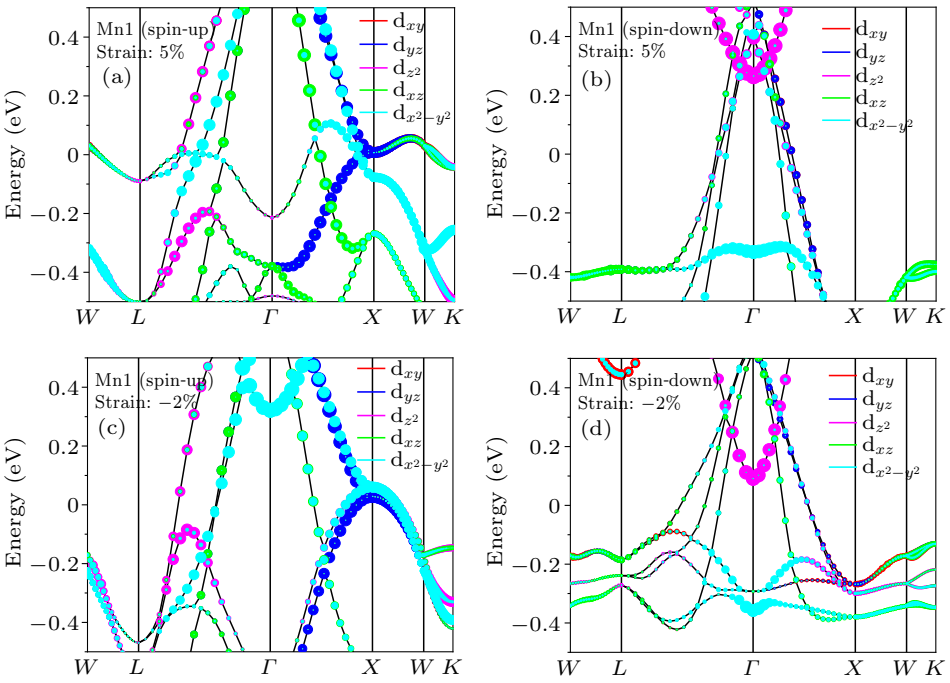


Fig. 16. The d-orbital-projected band structures of Mn1 in Mn_2FeIn under the different strain.

4. Conclusion

The electronic structure and magnetism of the Mn_2XIn (X = Fe, Co) Heusler compounds were studied over the range of strain between −2% and 5% by density functional calculations. Firstly, we predicted the crystal structure and magnetic properties, and found that both Mn_2FeIn and Mn_2CoIn belong to XA–I structures of the inverse Heusler compounds and have A-AFM ferromagnetic magnetism. Mn atoms have antiferromagnetic coupling between them. In addition, we calculated the structural stability of Mn_2XIn, determined the toughness of the two compounds, and found that their total magnetic moments remained at about 1.40 μ_B/f.u. and 1.69 μ_B/f.u., respectively. Under the biaxial strain, we observed that the DOS of Mn_2FeIn is sensitive to the biaxial strain, which is mainly manifested in the increase of spin polarization from −2% to 74%. The change of MA from [001] to [100] direction under strain can be ascribed to the hybridization of the $d_{x^2-y^2}/d_{xy}$ and d_{z^2}/d_{yz}orbitals.

Acknowledgements

Project supported by the Fundamental Research Funds for the Provincial Universities of Zhejiang Province, China (Grant No. GK229909299001-05) and Zhejiang Provincial Public Welfare Projects of China (Grant No. LGG22F030017).

References

[1] Belkharroubi F, Bourdim M, Maizia A, Belmiloud N, Khelfaoui F, Smahi Z, Boudia K, Benchehima M, Azzi S and Ameri M 2023 *Philos. Mag.* **103** 1090

[2] Belkharroubi F, Khelfaoui F, Amara K, Marbouh N, Ameri M and Abderrahmane Y S 2019 *Phys. Rev. B* **557** 56

[3] Wei X P, Cao T Y, Sun X W, Gao Q, Gao P F, Gao Z L and Tao X M 2020 *Chin. Phys. B* **29** 077105

[4] Graf T, Felser C and Parkin S S P 2011 *Prog. Solid State Chem.* **39** 1

[5] Zoubir M K, Fadila B, Keltoum B, Ibrahim A and Mohammed A 2021 *Mater. Test* **63** 537

[6] Azar S M, Hamad B A and Khalifeh J M 2012 *J. Magn. Magn. Mater.* **324** 1776

[7] Sarkar S and Bansal C 2004 *J. Alloys Compd.* **366** 107

[8] Sugihara A, Mizukami S, Yamada Y, Koike K and Miyazaki T 2014 *Appl. Phys. Lett.* **104** 132404

[9] Vinesh A, Bhargava H, Lakshmi N and Venugopalan K 2009 *J. Appl. Phys.* **105** 7307

[10] Ishida S, Kawakami S and Asano S 2004 *Mater. Trans.* **45** 1065

[11] Ishida S, Masaki T, Fujii S and Asano S 1998 *Physica B* **245** 1

[12] Kellou A, Feneneche N, Grosdidier T, Aourag H and Coddet C 2003 *J. Appl. Phys.* **94** 3292

[13] Luo H Z, Zhang H W, Zhu Z Y, Ma L, Xu S F, Wu G H, Zhu X X, Jiang C B and Xu H B 2008 *J. Appl. Phys.* **103** 225

[14] Groot R a D, Mueller F M, Engen P G V and Buschow K H J 1983 *Phys. Rev. Lett.* **50** 25

[15] Picozzi S, Continenza A and Freeman A J 2002 *Phys. Rev. B* **66** 94421

[16] Yoshio, Miura, Kazutaka, Nagao, Masafumi and Shirai 2004 *Phys. Rev. B* **69** 144413

[17] Amrich O, Monir M E A, Baltach H, Omran S B, Sun X W, Wang X, Al-Douri Y, Bouhemadou A and Khenata R 2018 *Journal of Superconductivity and Novel Magnetism* **31** 241

[18] Babalola M and Iyorzor B 2019 *J. Magn. Magn. Mater.* **491** 165560

[19] Chen Y, Wu B, Yuan H, Feng Y and Chen H 2015 *J. Solid State Chem.* **221** 311

[20] Patel P D, Pillai S B, Shinde S M, Gupta S D and Jha P K 2018 *Physica B* **550** 376

[21] Hamaya K, Itoh H, Nakatsuka O, Ueda K, Yamamoto K, Itakura M, Taniyama T, Ono T and Miyao M 2009 *Phys. Rev. Lett.* **102** 137204

[22] Chibueze T C, Ekuma C E, Raji A T, Ezema F I and Okoye C M I 2020 *J. Alloys Compd.* **848** 156186

[23] Zhang Z W and Xu Y L 2013 *Superlattices Microstruct.* **57** 19

[24] Wang W D, Yang C G, Bai L W, Li M L and Li W B 2018 *J. Nanomater* **8** 74

[25] Appel O, Breuer G, Cohen S, Beeri O and Zalkind S 2019 *Mater. Sci.* **12** 1509

[26] Bach P, Bader A S, Ruster C, Gould C and Heinrich B 2003 *Appl. Phys. Lett.* **83** 521

[27] Baral M, Chattopadhyay M K, Jangir R, Chakrabarti A and Ganguli T 2019 *J. Magn. Magn. Mater.* **475** 675
[28] Benatmane S and Cherid S 2020 *JETP Lett.* **111** 694
[29] Faleev S V, Ferrante Y, Jeong J, Samant M G, Jones B and Parkin S S P 2017 *Phys. Rev. B* **95** 045140
[30] Kresse G and Furthmüller J 1996 *Phys. Rev. B* **54** 11169
[31] Aravindan V, Rajarajan A K and Mahendran M 2021 *J. Electron. Mater.* **50** 1786
[32] Li Y, Xu P, Zhang X M, Liu G D, Liu E K and Li L W 2020 *Chin. Phys. B* **29** 087101
[33] Calandra M, Mazin I I and Mauri F 2009 *Phys. Rev. B* **80** 308
[34] Liu Y, Wang G, Huang Q S, Guo L W and Chen X L 2013 *Phys. Rev. Lett.* **110** 029603
[35] Mouhat F and Coudert F X 2014 *Phys. Rev. B* **90** 224104
[36] Wang J H, Zhang T T, Zhang Q W, Xia C, Wang W H, Qian S F, Cheng Z X, Zhang G and Wang X T 2024 *Adv. Funct. Mater.* **34** 2316079
[37] Li G J, Liu E K, Liu G D, Wang W H and Wu G 2021 *Chin. Phys. B* **30** 083103
[38] Wang X T, Zhao W Q, Cheng Z X, Dai X F and Khenata R 2018 *Solid State Commun.* **269** 125
[39] Xie H H, Gao Q, Li L, Lei G, Mao G Y, Hu X R and Deng J B 2015 *Comput. Mater. Sci.* **103** 52
[40] Yalcin B G and Bagci S 2015 *J. Phys. D: Appl. Phys.* **48** 475304
[41] Priyambada A and Parida P 2024 *J. Phys. Chem. Solids* **188** 111892
[42] Priyambada A, Deep R and Parida P 2024 *Comput. Condens. Matter* **39** e00893
[43] Gong J L, Wang Y, Han Y L, Cheng Z X, Wang X T, Yu Z M and Yao Y G 2024 *Adv. Mater.* **36** e2402232
[44] Liu J R, Wei X P, Chang W L and Tao X M 2022 *J. Phys. Chem. Solids* **163** 110600
[45] Khandy S A and Chai J D 2020 *J. Appl. Phys.* **127** 165102
[46] Wang V, Xu N, Liu J C, Tang G and Geng W T 2019 *Comput. Phys. Commun.* **267** 108033
[47] Reuss A 1929 *Appl. Math. Mech.* **9** 49
[48] Musari A A, Sunmonu R S and Babajide S O 2024 *Comput. Condens. Matter* **39** e00890
[49] Puthusseri N N and Natesan B 2024 *Comput. Condens. Matter* **39** e00894
[50] Grewal S, Surehli M K, Nag S and Kumar R 2024 *Comput. Condens. Matter* **39** e00910
[51] Galanakis I, Ph. D and Papanikolaou N 2002 *Phys. Rev. B* **66** 174429
[52] Epishin A I and Lisovenko D S 2016 *Tech. Phys.* **61** 1516
[53] Gercek H 2007 *Int. J. Rock Mech. Min. Sci.* **44** 1
[54] Güler E, Güler M, Uğur and Uğur G 2021 *Int. J. Quantum Chem.* **121** e26606
[55] Pettifor D 1992 *Mater. Sci. Technol.* **8** 345
[56] Friák M, Ob M and Vitek V 2003 *Philos. Mag.* **83** 3529
[57] Hao L, Khenata R, Wang X and Yang T 2019 *J. Electron.* **48** 6222
[58] Li X, Chen X, Meng C and Ji G 2006 *Solid State Commun.* **139** 197
[59] Al-Qaisi S, Abu-Jafar M S, Gopir G K, Ahmed R, Bin Omran S, Jaradat R, Dahliah D and Khenata R 2017 *Results Phys.* **7** 709
[60] Pauling and Linus 1938 *Phys. Rev. B* **54** 899
[61] Slater J C 1937 *J. Appl. Phys.* **8** 385
[62] Ahmad A, Srivastava S K and Das A K 2021 *J. Alloys Compd.* **878** 160341
[63] Aravindan V, Rajarajan A K, Vijayanarayanan V and Mahendran M 2022 *Funct. Mater. Lett.* **15** 2251011
[64] Benatmane S and Bouhafs B 2019 *Comput. Condens. Matter* **19** e00371
[65] Katubi K M, Shakil M, Pervaiz H, Gillani S, Gadhi M A, Ahmad S and Al-Buriahi M S 2023 *Indian J. Phys.* **97** 2669
[66] Rached H 2021 *Int. J. Quantum Chem.* **121** e26647
[67] Inomata K, Ikeda N, Tezuka N, Goto R, Sugimoto S, Wojcik M and Jedryka E 2008 *Sci. Technol. Adv. Mater.* **9** 014101
[68] Chen J R, Gong Y T, Lu X Y, Zhang C Y, Hu Y, Wang M Z, Shi Z, Fu S, Cai H L, Liu R B, Yuan Y, Lu Y, Liu T Y, You B, Xu Y B and Du J 2023 *Chin. Phys. Lett.* **40** 047501
[69] Hao R R, Zhang K, Li Y G, Cao Q, Zhang X Y, Zhu D P and Zhao W S 2022 *Chin. Phys. B* **31** 017502
[70] Forstreuter J, Steinbeck L, Richter M and Eschrig H 1997 *Phys. Rev. B* **55** 9415
[71] Odkhuu D 2016 *Phys. Rev. B* **94** 060403
[72] Wang X T, Li X P, Li J H, Xie C W, Wang J H, Yuan H K, Wang W H, Cheng Z X, Yu Z M and Zhang G 2023 *Adv. Funct. Mater.* **33** 2304499
[73] Gong J L, Ding G Q, Xie C W, Wang W H, Liu Y, Zhang G and Wang X T 2024 *Adv. Sci.* **11** e2307297
[74] Chen J L and Hu J 2024 *Chin. Phys. B* **33** 087502